

Effects of Sb on the Thermoelectric Properties of PbTe

Tao-Hsing Chen* and Ming-Tai Hong

Department of Mechanical Engineering, University of Kaohsiung University of Applied Sciences,
Kaohsiung 807, Taiwan

*E-mail: thchen@cc.kuas.edu.tw

Received: 03 August 2015 / Accepted: 29 August 2015 / Published: 30 September 2015

This study focuses on improving the thermoelectric properties of PbTe-based materials by adding different Sb content. The potential for achieving high thermoelectric efficiency in Sb-doped n-type PbTe-based thermoelectric compounds is described, and the electrical resistivity, Seebeck coefficient and thermal conductivity are measured from room temperature to about 500K. The effects of the Sb concentration in Sbx (Pb₁₈Te₂₀) on the resulting thermoelectric properties are studied. Furthermore, the surface features of Sbx (Pb₁₈Te₂₀) are also observed.

Keywords: Sb, thermoelectric Properties, PbTe, Seebeck coefficient

1. INTRODUCTION

Solid-state thermoelectric (TE) materials are attracting growing attention for their use in renewable energy and electronic cooling applications [1, 2]. The high performance of TE materials is quantified by their large figure of merit, ZT. The ZT is defined as $(S^2\sigma/\kappa)T$ [3-5], where S is the Seebeck coefficient, σ is electrical conductivity, $S^2\sigma$ is the power factor, and T is the absolute temperature.

One of the most thermoelectric materials is lead telluride (PbTe), which is suitable for use at medium temperatures, such as in power generation and cooling applications [1]. Recently, many studies have focused on doping PbTe with various elements to improve the carrier concentration and add some nanostructure materials to improve its TE performance [6]. One study [7] reported that the addition of Ag and Sb to PbTe produced a new quaternary TE material, which can obtain a ZT value above 1.7 at about 700K, due to the significant reduction in thermal conductivity, caused by the nanostructure of the PbTe matrix. This material has many desirable properties, such as an isotropic morphology, high

crystal symmetry, and the ability to control the carrier concentration. In contrast, the TE properties of non-doped PbTe are low because of their poor electrical conductivity.

There are many elements that can be added to PbTe materials, such as Ag, Sb, and Co. This study investigates the effects of adding different amounts of Sb to PbTe, and especially the TE properties of the resulting PbSb_xTe material. There are many methods that can be used to produce the PbTe materials, such as vacuum melting [8–11], a mechanical alloy method with hot pressing [12, 13], and vapor phase deposition [14]. In contrast to conventional melting, this study uses the vacuum arc melting method, which can both reduce the energy needed and be effective in limiting grain growth. Furthermore, the samples after vacuum arc melting have some pores in the surface. Therefore, it uses the electrochemical deposition method to make the more compact surface and good grain growth.

2. MATERIAL PREPARATION AND EXPERIMENTAL PROCEDURE

The Pb₁₈Sb_xTe₂₀ samples were prepared with commercial powders Sb (99.99%), Pb (99.9%) and Te (99.999% in-purity), which were weighed according to stoichiometry. After being uniformly mixed in an agate mortar in an atmosphere of argon, the specimens were formed by pressing. The pressed specimens were then put into a vacuum arc melting furnace. To obtain material with good TE properties, the alloy was melted three times at 873K for 12 hours and the pressure during the melting process is 1.3×10^{-3} torr. After vacuum arc melting, we put the samples into solution with Pb(NO₃)₂, H₂TeO₃ and Sb₂O₃ which are diluting the tartaric acid and HNO₃.

The phase structures were investigated by X-ray diffraction and the microstructure of all the samples was examined by SEM (Scanning Electron Microscopy). Finally, the Seebeck coefficient and electrical resistivity were measured by using a four-point direct current (dc) and commercial equipment, a (ZEM-3(M8) system. The thermal conductivity was calculated using the equation $k = \alpha C_p \rho$, where α is the thermal diffusivity, C_p is the heat capacity and ρ is the density.

3. RESULTS AND DISCUSSION

3.1. Analysis of Micro-structure

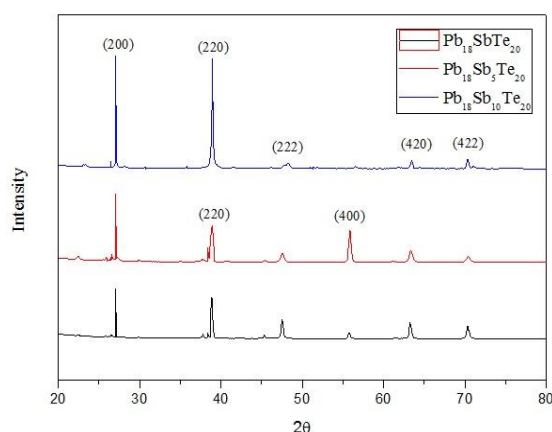
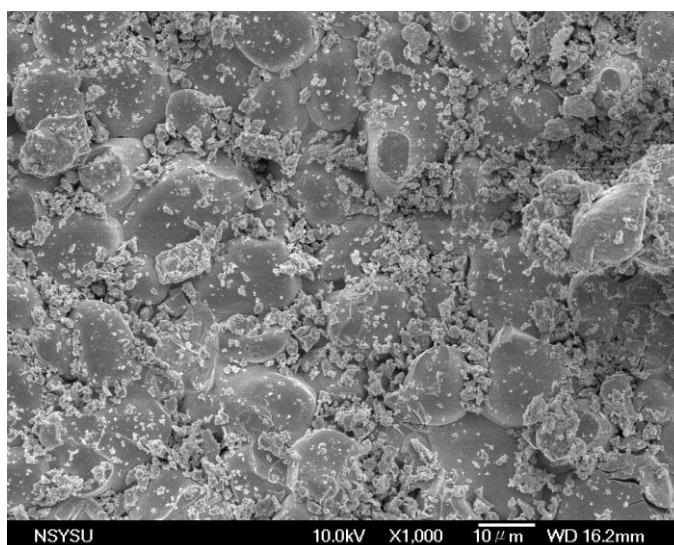
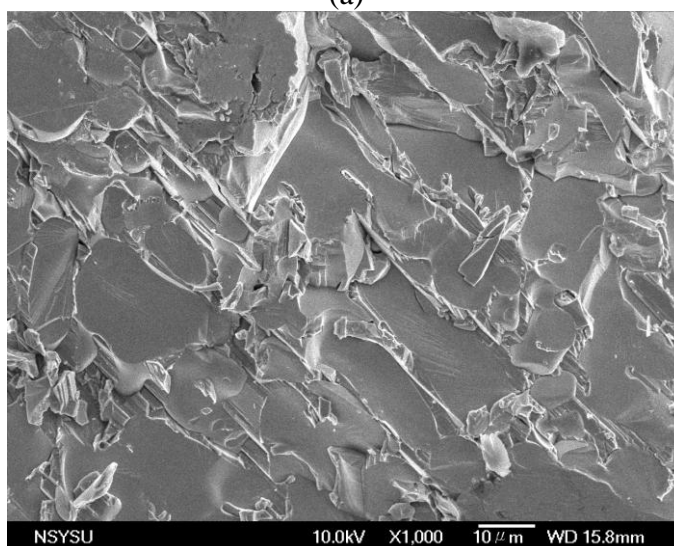


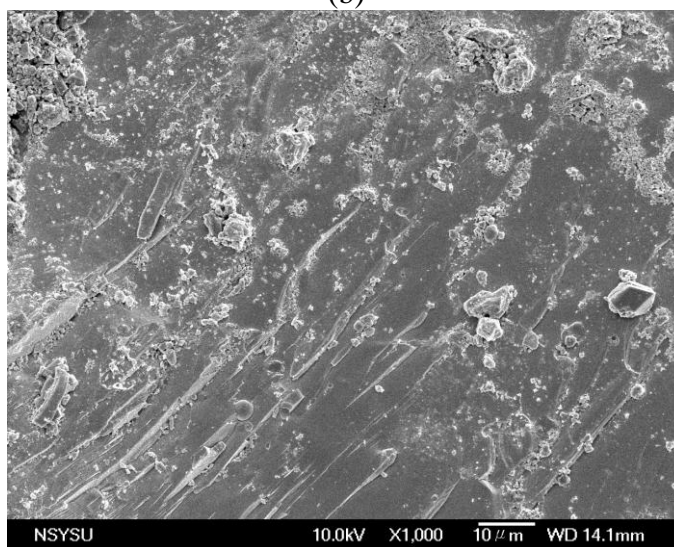
Figure 1. XRD diffraction patterns of the Pb₁₈Sb_xTe₂₀ (x=1, 5, 10).



(a)



(b)



(c)

Figure 2. SEM micrographs of the fracture surfaces of (a) $\text{Pb}_{18}\text{SbTe}_{20}$, (b) $\text{Pb}_{18}\text{Sb}_5\text{Te}_{20}$, and (c) $\text{Pb}_{18}\text{Sb}_{10}\text{Te}_{20}$.

The XRD spectra of $\text{Pb}_{18}\text{Sb}_x\text{Te}_{20}$ are shown in Figure 1. The XRD patterns of all samples are indexed very well with the standard diffraction of the PbTe structure (NaCl Fm3m symmetry structure). This indicates that the specimens prepared by the vacuum arc melting method are single phase PbTe.

Figures 2a-2c show typical SEM fracture surface micrographs of the $\text{Pb}_{18}\text{SbTe}_{20}$, $\text{Pb}_{18}\text{Sb}_5\text{Te}_{20}$ and $\text{Pb}_{18}\text{Sb}_{10}\text{Te}_{20}$ specimens prepared by the vacuum arc melting process. They reveal that all the specimens are very dense. Although grain boundaries are hardly to observe in the SEM photographs, it can be clearly seen that all the specimens have rather different textures. There are small striped structures in the $\text{Pb}_{18}\text{SbTe}_{20}$ specimen. When the Sb content is increased to 5%, it contains many long and curly stripes. However, the number of striped structures is less in the $\text{Pb}_{18}\text{Sb}_{10}\text{Te}_{20}$ specimen.

3.2. Electrical and Seebeck coefficient analysis

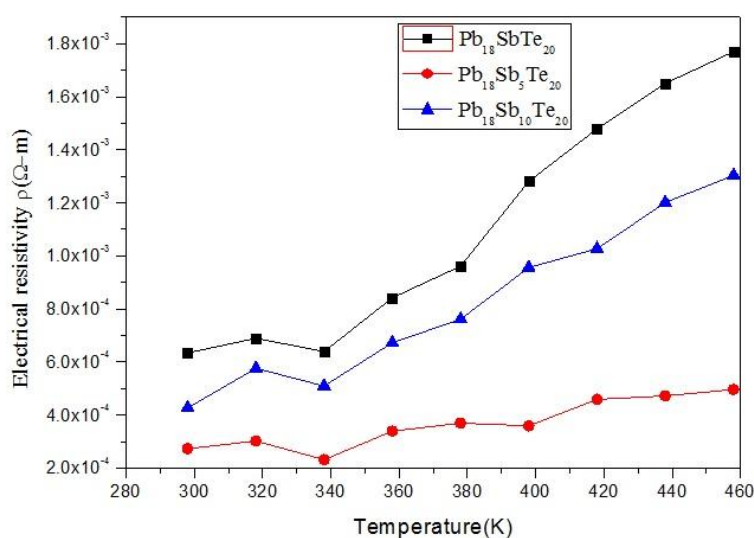


Figure 3. Electrical conductivity of $\text{Pb}_{18}\text{Sb}_x\text{Te}_{20}$ ($x=1, 5, 10$) as a function of temperature.

Figure 3 shows the electrical conductivity as a function of temperature for all the specimens. The electrical conductivity of the $\text{Pb}_{18}\text{Sb}_5\text{Te}_{20}$ specimens is lower than that of the $\text{Pb}_{18}\text{SbTe}_{20}$ and $\text{Pb}_{18}\text{Sb}_{10}\text{Te}_{20}$ specimens over the whole temperature range. However, the increased electrical resistivity with increasing temperature for all the specimens indicates that they are semiconductors

Figure 4 shows that the Seebeck coefficient for all three specimens is a function of temperature. The Seebeck coefficients are all positive, which indicates that the $\text{Pb}_{18}\text{Sb}_x\text{Te}_{20}$ specimens have p type behavior. Furthermore, the $\text{Pb}_{18}\text{Sb}_5\text{Te}_{20}$ specimen has the highest Seebeck coefficient compared to the others below 340K. After 340K the Seebeck coefficient of $\text{Pb}_{18}\text{Sb}_5\text{Te}_{20}$ becomes negative, although the absolute value remains higher than those of the other specimens. A negative value means that the dominant carriers change from electronic holes to electrons as the experimental temperature increases, which corresponds with the results reported by Orihashi *et al* [15]. There are some studies present the

negative value of Seebeck coefficient in the whole temperature range which indicates the n-type conduction in [16, 17]

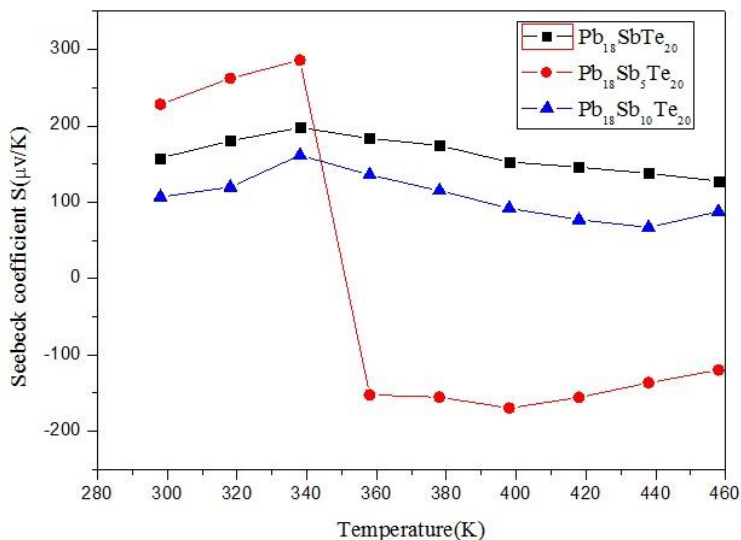


Figure 4. The Seebeck coefficients of the specimens with different Sb content.

3.3. Thermoelectric properties

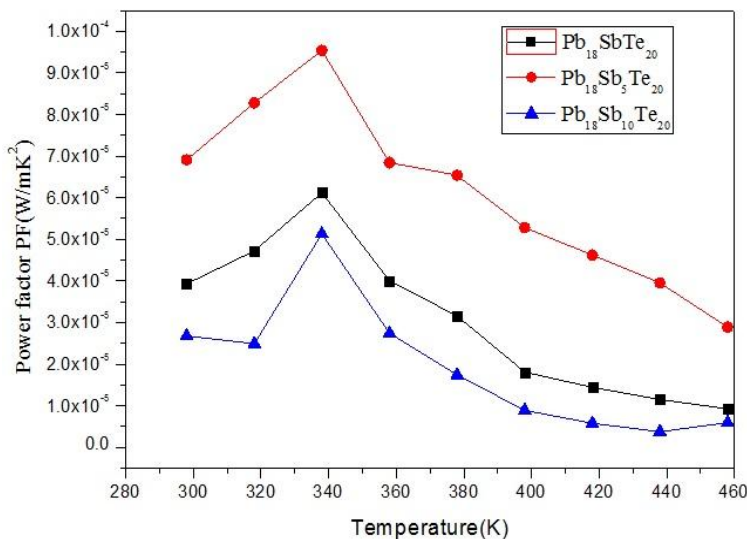


Figure 5. The power factor for all specimens at different temperature.

It presents the temperature dependence of the power factor in Figure 5 for the Pb₁₈Sb_xTe₂₀ specimens, which is calculated from the measured electrical conductivity and Seebeck coefficient. The power factor of the specimens increased along with the temperature up to 340K. However, at temperatures higher than 340K, the value of the power factor decreases. Furthermore, the power factor of the Pb₁₈Sb₅Te₂₀ specimen was higher than that of the other Sb specimens throughout the whole

measured temperature range. This greater power factor is attributed to the mainly increase in the electrical conductivity without any mainly decrease in the Seebeck coefficient.

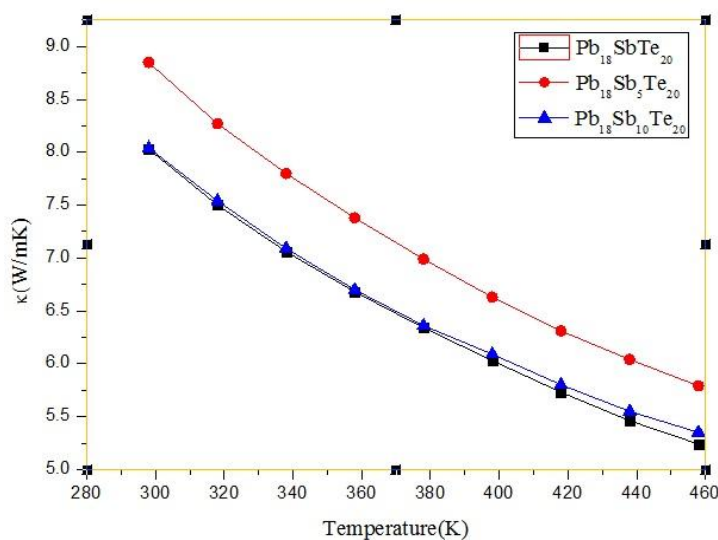


Figure 6. Variations in thermal conductivity with temperature for $\text{Pb}_{18}\text{Sb}_x\text{Te}_{20}$ ($x=1, 5$ and 10).

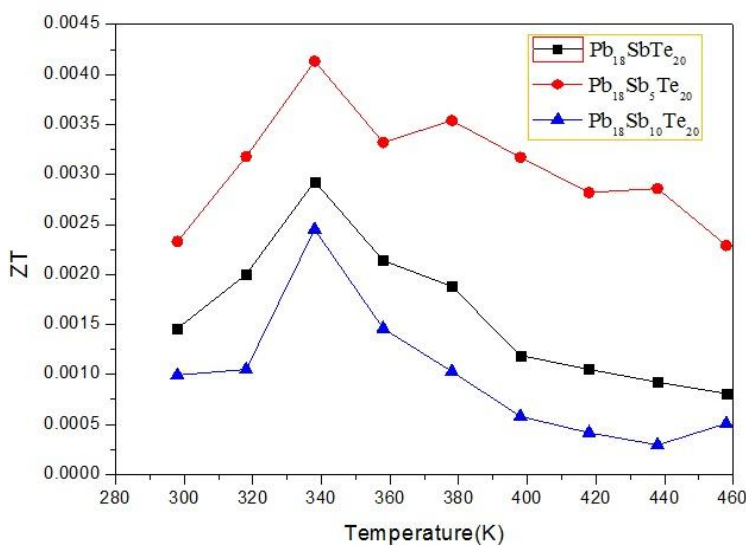


Figure 7. The ZT values as a function of temperature for all the $\text{Pb}_{18}\text{Sb}_x\text{Te}_{20}$ specimens ($x = 1, 5$ and 10).

Figure 6 shows the thermal conductivity for the $\text{Pb}_{18}\text{Sb}_x\text{Te}_{20}$ ($x = 1, 5$ and 10) specimens as a function of temperature. It can be seen that for all specimens the thermal conductivity decreases as the temperature and Sb content increases. However, when the Sb content was 10%, the thermal conductivity decreased. This is similar to the results found for the electrical properties, and the $\text{Pb}_{18}\text{Sb}_5\text{Te}_{20}$ specimen has the highest electrical conductivity, and thus the highest electrical thermal conductivity.

The values of ZT are calculated from the electrical resistivity, thermal conductivity and Seebeck coefficient. Figure 7 is shown that the calculated values of ZT for all specimens. The maximum ZT value amongst all samples is 0.004 at 340 K, which is mainly due to the lowest electrical resistivity. It is therefore, obvious that 5% is the best content of Sb in $\text{Pb}_{18}\text{Sb}_x\text{Te}_{20}$.

4. CONCLUSION

The $\text{Pb}_{18}\text{Sb}_x\text{Te}_{20}$ specimens used in this study were prepared by vacuum arc melting. The thermoelectric characteristics were measured from 280K to 460K. The results show that both the electrical resistivity and the absolute value of the Seebeck coefficient increase along with the temperature. In contrast, the thermal conductivity decreases as the temperature increases. Furthermore, the best TE properties are obtained when the Sb content is 5%. The figure of merit, i.e., the ZT value, for $\text{Pb}_{18}\text{Sb}_5\text{Te}_{20}$ is 0.004 at 340K.

ACKNOWLEDGEMENTS

This work was supported by the Ministry of Science and Technology (MST) of Taiwan under contract no. NSC 102-2212-E-151-006-MY3

References

1. T. Su, X. Jia, H. Ma, J. Guo, Y. Jiang, N. Donga, L. Deng, X. Zhao, T. Zhu and C. Wei, *J. Alloy Compd.*, 468 (2009) 410.
2. D.M. Rowe, *Thermoelectric Handbook: Macro to Nano*, Taylor & Francis, New York (2006).
3. A. Majumdar, *Science*, 303 (2004) 777.
4. D.Y. Chung, T. Hogan, P. Brazis, M. Rocci-Lane, C. Kannewurf, M. Bastea, C. Uher and M.G. Kanatzidis, *Science*, 287 (2000) 1024.
5. G.J. Snyder and E.S. Toberer, *Nat Mater.*, 7 (2008) 105–114.
6. S. Park, S. J. Tark and D. Kim, *Curr Appl Phys.*, 11 (2011) 1299.
7. M.K. Han, K. Hoang, H.J. Kong, R. Pcionek, C. Uher, K.M. Paraskevopoulos, S.D. Mahanti and M.G. Kanatzidis, *Chem Mater.*, 20 (2008) 3512.
8. Z.Y. Li, M. Zou and J.F. Li, *J. Alloy Compd.*, 549 (2013) 319.
9. G.E. Smith and R. Wolfe, *Appl Phys.*, 33 (1962) 841.
10. Y. Hor and R. Cava, *J Alloy Compd.*, 479 (2009) 368.
11. H. Noguchi, H. Kitagawa, T. Kiyabu, K. Hasezaki and Y. Noda, *Phys. Chem Solids*, 68 (2007) 91.
12. A. Kosuga, M. Uno, K. Kurosaki and S. Yamanaka, *J Alloy Compd.*, 391 (2005) 288.
13. H. Wang, J.F. Li, C.W. Nan, M. Zhou, W.S. Liu, B.P. Zhang and T. Kita, *Appl Phys Lett.*, 88 (2006) 092104.
14. M.L. Chang, M.S. Jeng, Y.W. Chou, J.R. Ku and B.H. Chen, *J. Alloy Compd.*, 509 (2011) 4089.
15. M. Orihashi, Y. Noda, L.D. Chen, T. Goto and T. Hirai, *J. Phys. Chem. Solids*, 61 (2000) 919.
16. S.V. Ovsyannikov and V.V. Shchennikov, *Appl. Phys. Lett.*, 90 (2007) 122103.
17. K.F. Cai, C. Yan, Z.M. He, J.L. Cui, C. Stiewe, E. Müller and H. Li, *J. Alloys Compd.* 469(2009) 499.